

Structural and doping effects in the half-metallic double perovskite $A_2\text{CrWO}_6$

J. B. Philipp,* P. Majewski, L. Alff,† A. Erb, and R. Gross
*Walther-Meißner-Institut, Bayerische Akademie der Wissenschaften,
 Walther-Meißner Str. 8, 85748 Garching, Germany*

T. Graf and M. S. Brandt
Walter-Schottky-Institut, TU München, Am Coulombwall 3, 85748 Garching, Germany

J. Simon, T. Walther, and W. Mader
Institut für Anorganische Chemie, Universität Bonn, Römerstr. 164, 53117 Bonn, Germany

D. Topwal and D. D. Sarma
Solid State and Structural Chemistry Unit, Indian Institute of Science, Bangalore 560 012, India
 (Dated: 19th July 2018)

The structural, transport, magnetic and optical properties of the double perovskite $A_2\text{CrWO}_6$ with $A = \text{Sr, Ba, Ca}$ have been studied. By varying the alkaline earth ion on the A site, the influence of steric effects on the Curie temperature T_C and the saturation magnetization has been determined. A maximum $T_C = 458\text{ K}$ was found for Sr_2CrWO_6 having an almost undistorted perovskite structure with a tolerance factor $f \simeq 1$. For Ca_2CrWO_6 and Ba_2CrWO_6 structural changes result in a strong reduction of T_C . Our study strongly suggests that for the double perovskites in general an optimum T_C is achieved only for $f \simeq 1$, that is, for an undistorted perovskite structure. Electron doping in Sr_2CrWO_6 by a partial substitution of Sr^{2+} by La^{3+} was found to reduce both T_C and the saturation magnetization M_s . The reduction of M_s could be attributed both to band structure effects and the Cr/W antisites induced by doping. Band structure calculations for Sr_2CrWO_6 predict an energy gap in the spin-up band, but a finite density of states for the spin-down band. The predictions of the band structure calculation are consistent with our optical measurements. Our experimental results support the presence of a kinetic energy driven mechanism in $A_2\text{CrWO}_6$, where ferromagnetism is stabilized by a hybridization of states of the nonmagnetic W-site positioned in between the high spin Cr-sites.

I. INTRODUCTION

The investigation of ordered double perovskite materials $A_2BB'\text{O}_6$ with A an alkaline earth such as Sr, Ba, or Ca and B, B' two different transition metals has been strongly stimulated by the discovery of a large room temperature magnetoresistive effect at low magnetic fields in $\text{Sr}_2\text{FeMoO}_6$ [1]. The fact that the double perovskites seem to be ferromagnetic metals with high Curie temperatures T_C of up to 635 K [2] and apparently have highly spin polarized conduction band makes these materials interesting for applications in spintronic devices such as magnetic tunnel junctions or low-field magnetoresistive sensors [3]. However, the double perovskites are also of fundamental interest since both their basic physics and materials aspects are not well understood.

It is evident that intensive research has been dedicated to both the variation of the metallic/magnetic ions on the B - and B' -site as well as electron doping studies, where the divalent alkaline earth ions on the A -site are partially replaced by a trivalent rare earth ion such as La, in order to understand the electronic structure and

the magnetic exchange in the double perovskites in detail. Furthermore, these studies aimed for the tailoring and optimization of the magnetic properties of the double perovskites for their use in magnetoelectronic devices such as spin valves, magnetic information storage systems, or as sources for spin polarized electrons in spintronics. Here, important aspects are the achievement of sufficiently high values for T_C and the spin polarization to allow for the operation of potential devices at room temperature. Along this line, in the compound $\text{Sr}_2\text{CrReO}_6$ a Curie temperature of $T_C = 635\text{ K}$ has been obtained [2]. Furthermore, in $\text{Sr}_2\text{FeMoO}_6$ an increase in T_C of about 70 K has been reported as a result of electron doping by partial substitution of divalent Sr^{2+} by trivalent La^{3+} [4]. With respect to magnetoresistance, up to now large low-field magnetoresistive effects have been found not only in $\text{Sr}_2\text{FeMoO}_6$ [1, 5, 6], but also in many other double perovskites as for example $\text{Sr}_2\text{FeReO}_6$ [7], Sr_2CrWO_6 [8], and $(\text{Ba}_{0.8}\text{Sr}_{0.2})_{2-x}\text{La}_x\text{FeMoO}_6$ [9].

The origin of magnetism in the double perovskite still is discussed controversially. Historically, the ferrimagnetism in the system $\text{Sr}_2\text{FeMoO}_6$ has been explained in terms of an antiferromagnetic superexchange interaction between the Mo^{5+} ($5d^1$) spin and the Fe^{3+} ($3d^5$) spins [10, 11, 12]. However, more recently Moritomo *et al.* found a strong correlation between the room temperature conductivity and the Curie temperature, implying that

*Electronic address: Boris.Philipp@wmi.badw.de

†Electronic address: Lambert.Alff@wmi.badw.de

the mobile conduction electrons mediate the exchange interaction between the local Fe^{3+} spins [13, 14]. Therefore, in analogy to the doped manganites it was tempting to explain the ferromagnetic coupling between the Fe sites based on a double exchange mechanism, where the delocalized electron provided by the Mo $4d^1$ configuration plays the role of the delocalized e_g electron in the manganites. However, as pointed out by Sarma [15] there are important differences between the manganites and the double perovskites. In the former, both the localized Mn t_{2g} electrons and the delocalized Mn e_g electron reside at the same site and their spins are coupled ferromagnetically by a strong on-site Hund's coupling. In the latter, the localized Fe $3d$ electrons (Fe^{3+} : $3d^5, S = 5/2$) and the delocalized Mo $4d$ electron (Mo^{5+} : $4d^1, S = 1/2$) nominally are at two different sites although the Mo $4d$ electron obtains a finite Fe character by sizable hopping interaction. At first glance this seems to support a double exchange scenario. However, in $\text{Sr}_2\text{FeMoO}_6$ according to band structure calculations the Fe $3d$ spin-up band is completely full making it impossible for another spin-up electron to hop between Fe sites and thus forcing the delocalized electrons to be spin-down electrons. Therefore, the Hund's coupling strength, which provides the energy scale for the on-site spin coupling in the double exchange mechanism for the manganites, cannot be invoked for $\text{Sr}_2\text{FeMoO}_6$. This demonstrates that in the double perovskites the antiferromagnetic coupling between the localized and the delocalized electrons, which according to the large T_C is strong, must originate from another mechanism. Such mechanism has been proposed by Sarma [15] for $\text{Sr}_2\text{FeMoO}_6$ and extended to many other systems by Kanamori and Terakura [16, 17]. In this model, the hybridization of the Mo $4d$ (t_{2g}) and Fe $3d$ (t_{2g}) states plays the key role in stabilizing ferromagnetism at high Curie temperatures [15, 16, 17]. If the Fe^{3+} spins are ferromagnetically ordered, the hybridization between the Fe $3d$ (t_{2g}) and the Mo $4d$ (t_{2g}) states pushes up and down the Mo $4d_{\uparrow}$ and Mo $4d_{\downarrow}$ states, respectively. The essential point in this scenario, which is discussed in more detail below, is that the hybridized states are located energetically between the exchange-split Fe $3d_{\uparrow}$ and the Fe $3d_{\downarrow}$ levels. We note that in this model the magnetic moment at the Mo site is merely induced by the Fe magnetic moments through the hybridization between the Fe $3d$ and the Mo $4d$ states what can be considered as a magnetic proximity effect. In this sense the double perovskites should be denoted ferromagnetic and not ferrimagnetic [18].

Despite the recent progress in understanding the physics of the double perovskites there is still an open debate on the adequate theoretical modelling. In particular, the details of the interplay between structural, electronic, and magnetic degrees of freedom in the double perovskites is not yet clearly understood. Recently, the T_C in double perovskites was discussed to depend sensitively on the band structure and band filling in contrast to experimental results [19]. However, since in experi-

ments often changes in the number of conduction electrons achieved by partially replacing the divalent alkaline earth ions on the A - and A' -site by trivalent rare earth ions are accompanied by significant steric effects, it is difficult to distinguish between doping and structural effects. It is therefore desirable to investigate both the influence of structural changes (changes in the bond length and bond angles) and the effect of carrier doping.

Here, we present a study of the effect of structural changes and doping in the double perovskite $A_2\text{CrWO}_6$ ($A = \text{Sr}, \text{Ba}, \text{Ca}$) on the magnetotransport, the magnetic and optical properties together with band structure calculations. We note that a major difference between the system $A_2\text{CrWO}_6$ and the systems $A_2\text{FeMoO}_6$ or $A_2\text{FeReO}_6$ is the fact that in the former the majority spin band is only partially filled ($\text{Cr}^{3+}, 3d^3, S = 3/2$, only the Cr $3d$ (t_{2g}) levels are occupied), whereas in the latter the majority spin band is completely filled ($\text{Fe}^{3+}, 3d^5, S = 5/2$, both the Fe $3d$ (t_{2g}) and Fe $3d$ (e_g) levels are occupied). We discuss that despite this difference the magnetism in $A_2\text{CrWO}_6$ and $A_2\text{FeMoO}_6$ is similar. For both systems the exchange gap is important for the magnetic exchange and half metallicity. However, whereas for the former system also the crystal field gap between the t_{2g} and the e_g levels plays a key role, for the latter the crystal field gap is irrelevant. A key result of our study is that optimum magnetic properties such as half metallicity and high T_C can only be obtained in the undoped compounds close to the ideal undistorted perovskite structure that is characterized by a tolerance factor $f \simeq 1$ of the perovskite unit cell. Furthermore, we find that electron doping tends to decrease T_C in $A_2\text{CrWO}_6$.

II. SAMPLE PREPARATION

In our study, we have used both polycrystalline and epitaxial thin film samples. Polycrystalline samples were prepared from stoichiometric mixtures of SrCO_3 , BaCO_3 , CaCO_3 , Cr_2O_3 , La_2O_3 , and WO_3 with a purity ranging between 99.99% and 99.999%. These powders were thoroughly mixed, placed in Al_2O_3 crucibles, and then repeatedly heated in a thermobalance under reducing atmosphere (H_2/Ar : 5%/95%) with intermediate grinding. The final sintering temperatures T_{sint} were increased from 1200°C for the first up to 1550°C for the final firing for the first series of samples. In order to increase the Curie temperature we prepared a second series of undoped Sr_2CrWO_6 samples with more sintering steps and longer final sintering times at lower (1300°C) temperatures. For this series we find the highest Curie temperatures, which correspond to the values reported in literature. This most likely is caused by a slightly higher oxygen content in these samples compared to those sintered at higher temperatures in the same reducing atmosphere. The use of the thermobalance allowed to monitor the ongoing reaction process due to the associated weight loss

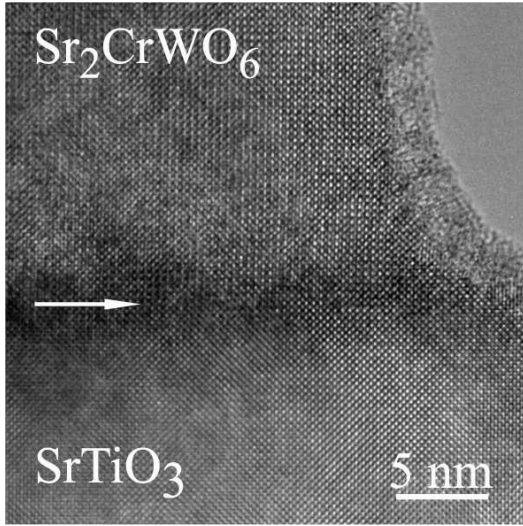


Figure 1: Transmission electron micrograph of an epitaxial Sr_2CrWO_6 thin film deposited on a SrTiO_3 substrate with low lattice mismatch ($\simeq 0.13\%$). The image was taken along the $[010]$ direction.

of the samples. The exact oxygen content of the investigated samples has not been determined. However, due to the very similar preparation procedure for the samples used for the study of electron doping, we can assume a similar oxygen content.

The polycrystalline samples were characterized by x-ray powder diffractometry to detect parasitic phases, e.g. the insulating compound SrWO_4 . Interestingly, even in samples containing SrWO_4 no chromium containing parasitic phases could be detected. The most simple explanation for this observation is the high vapor pressure of Cr_2O_3 resulting in a loss of chromium. However, no weight loss has been found in the thermogravimetric measurement. Therefore, it is more likely that the formation of the mixed phase $A_2\text{Cr}_{1+x}\text{W}_{1-x}\text{O}_{6\pm\delta}$ compensates for the missing Sr and W due to the SrWO_4 impurity phase. While the double perovskite $\text{Sr}_2\text{FeMoO}_6$ can be grown as single crystal [20, 21, 22], our attempts to grow single crystals of Sr_2CrWO_6 by floating zone melting failed so far due to the high vapor pressure of Cr_2O_3 at the melting point.

Epitaxial thin films of Sr_2CrWO_6 were fabricated in a UHV Laser molecular beam epitaxy (L-MBE) system [23]. The details of the thin film deposition have been described recently [8, 24]. Fig. 1 shows a transmission electron micrograph of an epitaxial Sr_2CrWO_6 thin film grown on a SrTiO_3 (001) substrate. The image shows that the thin film grows epitaxially with high crystalline quality. The c -axis oriented films have been analyzed using a high resolution 4-circle x-ray diffractometer. Only (00ℓ) peaks could be detected and typically, rocking curves of the (004) peak had a full width at half maximum (FWHM) of only 0.02 to 0.03°, which is very close to the FWHM of the substrate peak. Moreover, an AFM

analysis of the Sr_2CrWO_6 films showed that they have a very small surface roughness of the order of one unit cell [24]. In this study the thin films were used for optical measurements in order to determine the band structure.

III. EXPERIMENTAL RESULTS AND DISCUSSION

A. Structural Properties

It is well known that the tolerance factor f determines the crystal structure of perovskites $AB\text{O}_3$ [25]. Only for f close to unity a cubic perovskite structure is obtained. For $f \neq 1$ a tilt and rotation of the oxygen octahedra is obtained compensating for the misfit of the ionic radii of the involved A and B cations. Hence, the deviation of the tolerance factor from the ideal value $f = 1$ can be used as a measure for the internal strain in perovskites induced by the different radii of the A and B cations. This can be seen from the definition of f given by

$$f = \frac{r_A + r_O}{\sqrt{2}(\langle r_B \rangle + r_O)}.$$

Here, $\langle r_B \rangle$ denotes the average ionic radius for the ions on the B -site. For $f < 1$, the strain is compensated by a tilt and rotation of the oxygen octahedra. This results in a deviation of the $B\text{-O}\text{-}B$ bond angles from the ideal value of 180°. For $0.96 \leq f \leq 1$ the connecting pattern of the oxygen octahedra is rhombohedral, whereas it is orthorhombic for lower values of f [26]. A simple consequence of the deviation of the bond angles from 180° is a decrease in the hopping amplitude because the electron transfer between the B sites is via O 2p-states. This, in turn, results in a decrease of the one-electron bandwidth W . For $f > 1.06$, a hexagonal structure is expected which is classified by the stacking sequence of the BO_6 octahedra [28].

In the following, we discuss the change of tolerance factor f and its influence on the structure for the system $A_2\text{CrWO}_6$ with $A = \text{Sr, Ba, Ca}$. An overview on the crystallographic properties of the investigated samples is given in Table I. We note that samples with mixed contents of different alkaline earth ions on the A -site had a strong tendency to phase separation and are therefore excluded from our analysis. The value of f was calculated using the bond valence parameters as obtained using the SPuDS simulation software [29]. While Sr_2CrWO_6 has an almost ideal tolerance factor $f \simeq 1$, for Ca_2CrWO_6 the tolerance factor is much smaller ($f = 0.945$), and much larger than 1 ($f = 1.059$) for Ba_2CrWO_6 . The crystal structure of the different compounds was determined by a Rietveld refinement of the x-ray data. The result of the refinement is listed in Table I. As expected, the Sr_2CrWO_6 compound with $f = 0.999$ is cubic. In contrast, the Ca_2CrWO_6 compound with $f = 0.945$ is strongly distorted forming a monoclinic system as predicted by the SPuDS program [29]. The Ba_2CrWO_6 com-

Table I: Overview on the crystallographic properties of the investigated samples of the $A_2\text{CrWO}_6$ series with $A = \text{Sr}, \text{Ba}, \text{Ca}$. The tolerance f factor was calculated using the SPuDS simulation software [29].

material	structure	f	parasitic phases
T_{int}	bond angle, lattice parameters		
Ca_2CrWO_6	$P2_1/n$, $\beta = 90.1^\circ$, $a = 5.39 \text{ \AA}$	0.945	CaWO_4
1400°C	$b = 5.45 \text{ \AA}$, $c = 7.66 \text{ \AA}$		
	$a_{\text{pseudocubic}} = 7.66 \text{ \AA}$		
	antisites Cr/W: 13%		
Sr_2CrWO_6	$Fm\bar{3}m$, $a = 7.82 \text{ \AA}$	0.999	
1550°C	antisites Cr/W: 23%		SrWO_4
1300°C	antisites Cr/W: 31%		Sr_2WO_5
Ba_2CrWO_6	$P\bar{6}2c$, $a = 5.70 \text{ \AA}$, $c = 13.99 \text{ \AA}$	1.059	Ba_3WO_6
1450°C	$a_{\text{pseudocubic}} = 8.06 \text{ \AA}$		
	B_1 sites: 75% Cr and 25% W		
	B_2 sites: 100% W		

ound with $f = 1.059$ has a 6-layered hexagonal structure. The pseudocubic lattice parameter for Ba_2CrWO_6 is about 8.06 Å. The crystal structure is identical to that of the compound $\text{Ba}_3\text{Cr}_2\text{WO}_9$, where the B sites are not equivalent. Two third of the sites are centered within face-shared octahedra (B_1 site), whereas one third is centered within corner-shared octahedra (B_2 site) [28].

Antisite defects can occur if Cr and W ions exchange their positions on the B and B' sublattices. If Cr and W are randomly distributed, antisites are 50%. The amount of Cr/W antisites has been determined by a Rietveld refinement of the x-ray data. We first discuss the Sr_2CrWO_6 compound for which the amount of antisites is 23%. This value is higher than that obtained for the Fe/Mo system [6]. This most likely is caused by the much smaller difference in the ionic radii [27] between the Cr ($r_{\text{Cr}^{3+}} = 0.615 \text{ \AA}$) and W ($r_{\text{W}^{5+}} = 0.62 \text{ \AA}$) ions compared to the significantly larger difference between the Fe ($r_{\text{Fe}^{3+}}$, high spin = 0.645 Å) and Mo ($r_{\text{Mo}^{5+}} = 0.61 \text{ \AA}$) ions. In general, the amount of antisites on the B and B' sublattices is reduced by both large differences in the ionic radius and the valence state. Therefore, in the $\text{Cr}^{2+}/\text{W}^{6+}$ system ($r_{\text{Cr}^{2+}} = 0.73 \text{ \AA}$ and $r_{\text{W}^{6+}} = 0.60 \text{ \AA}$) the amount of antisites is reduced compared to the $\text{Cr}^{3+}/\text{W}^{5+}$ system. The measured small amount (23%) of antisites in Sr_2CrWO_6 suggests an intermediate valence state.

The amount of Cr/W antisites in the Ca_2CrWO_6 compound was determined to about 13%. The lower amount of antisites in Ca_2CrWO_6 (see Table I) may be associated with a gradual transition from W^{5+} to W^{6+} . The situation for the Ba_2CrWO_6 compound is more difficult. While in $\text{Ba}_3\text{Cr}_2\text{WO}_9$ the Cr and W ions each are located only on one sort of B site, this is not the case for Ba_2CrWO_6 . The Rietveld refinement shows that the W ions are occupying almost completely the B_2 sites. The

rest of the W ions and the Cr ions is located on the B_1 sites. A possible order of W and Cr ions on the B_1 sites was not considered in our analysis.

We briefly compare the crystallographic properties of the $A_2\text{CrWO}_6$ systems to those of other double perovskites. For the system $A_2\text{FeMoO}_6$ the use of different alkaline earth ions on the A site results in the following crystal structures: $\text{Ca}_2\text{FeMoO}_6$ with $f = 0.954$ is monoclinic or orthorhombic, $\text{Sr}_2\text{FeMoO}_6$ with $f = 1.009$ is about cubic (with very small tetragonal distortion), and $\text{Ba}_2\text{FeMoO}_6$ with $f = 1.06$ is cubic [30, 31, 32, 33]. We note, however, that the system is on the brink of a structural phase transition as a function of f . The $\text{Ba}_2\text{FeMoO}_6$ compound is close to a hexagonal structure. From the collected data listed in Table II we can formulate the following empirical rule: For $0.96 \lesssim f \lesssim 1.06$ in the majority of cases the double perovskites are cubic/tetragonal. For $f \lesssim 0.96$, orthorhombic/monoclinic structures are favored, whereas for $1.06 \lesssim f$ a hexagonal structure is preferred. Note, that the doped manganites of the most intensively investigated composition $\text{La}_{2/3}^{3+}A_{1/3}^{2+}\text{MnO}_3$ have $f \lesssim 0.95$ depending little on the chosen coordination number [34, 35]. It is therefore obvious that structural distortions play a more severe role in the manganites that are close to a metal-insulator-transition.

B. Transport Properties

Fig. 2 shows the temperature dependence of the resistivity for the double perovskites $A_2\text{CrWO}_6$ with $A = \text{Sr}, \text{Ba}, \text{Ca}$. All samples show an increase of the resistivity with decreasing temperature. Since the investigated samples are polycrystalline, the influence of grain boundaries plays an important role. Hence, the observed semiconductor like resistivity vs temperature curves may be related to the grain boundary resistance, whereas the intrinsic resistance of the double perovskites may be metallic. Although the intrinsic resistivity behavior cannot be unambiguously derived from our measurements, the fact that $d \ln \sigma / d \ln T \rightarrow 0$ for $T \rightarrow 0$ (see inset of Fig. 2) provides significant evidence for a metallic behavior in the Sr_2CrWO_6 sample. Here, σ is the electrical conductivity. The observed trend that the resistivity increases, if Sr_2 is replaced by Ca_2 and even more by Ba_2 , can be understood as follows: In contrast to the cubic perovskite Sr_2CrWO_6 , Ca_2CrWO_6 has a distorted perovskite structure with a B -O- B bonding angle deviating from 180°. This result in a reduction of the overlap between the relevant orbitals and, hence, the hopping amplitude. Finally, the Ba_2CrWO_6 compound has the highest resistivity most likely due to its hexagonal structure (see Table I).

The magnetotransport properties of Sr_2CrWO_6 already has been discussed elsewhere [8]. We found, that polycrystalline samples containing a large number of grain boundaries show a large negative low-field magne-

Table II: Structure, tolerance factor, and magnetic properties of various double perovskites. The tolerance f factor was calculated using the SPuDS simulation software [29].

material	crystallographic structure lattice parameters [Å]	f	magnetic order T_C or T_N [K]	$M_{\text{sat}}(5\text{K})$ (μ_B /f.u.)	$MR @ 50\text{kOe}$ [%]
$\text{Ca}_2\text{CrMoO}_6$	orthorhombic, $a = 5.49$ $b = 5.36$, $c = 7.70$ [36]	0.954 (3+/5+)	$T_C = 148$ [36]		
$\text{Sr}_2\text{CrMoO}_6$	$Fm\bar{3}m$, $a = 7.84$ [37]	1.009 (3+/5+)	$T_C = 450$ [37]	0.5 [13]	-5 (40 K) [37]
$\text{Ba}_2\text{CrMoO}_6$		1.070 (3+/5+)			
$\text{Ba}_3\text{Cr}_2\text{MoO}_9$	$P6_3/mmc$, $a = 5.69$, $c = 1.39$ [28]		paramagnetic [28]		
$\text{Ca}_2\text{CrReO}_6$	$P2_1/n$, $a = 5.38$, $b = 5.46$ $c = 7.65$, $\beta = 90^\circ$ [2]	0.952 (3+/5+)	$T_C = 360$ [2]	0.82 [2]	
$\text{Sr}_2\text{CrReO}_6$	$I4/mmm$, $a = 5.52$, $c = 7.82$ [2]	1.006 (3+/5+)	$T_C = 635$ [2]	0.86 [2]	
$\text{Ba}_2\text{CrReO}_6$		1.067 (3+/5+)			
$\text{Ba}_3\text{Cr}_2\text{ReO}_9$	hexagonal, $a = 4.94$, $c = 13.8$ [38]				
Ca_2CrWO_6	$P2_1/n$, $a = 5.39$, $b = 5.45$ $c = 7.66$, $\beta = 90.1^\circ$	0.945 (3+/5+)	$T_C = 161$	1.34	-9
Sr_2CrWO_6	$Fm\bar{3}m$, $a = 7.82$	0.99 (3+/5+)	$T_C = 458$	1.11	-48
Ba_2CrWO_6	$P\bar{6}2c$, $a = 5.70$, $c = 13.99$	1.059 (3+/5+)	$T_C = 145$	0.02	0
$\text{Ba}_3\text{Cr}_2\text{WO}_9$	$P\bar{6}2c$, $a = 5.69$, $c = 13.99$ [28]		paramagnetic [28]		
$\text{Sr}_2\text{MnMoO}_6$	$Fm\bar{3}m$, $a = 8.01$ [13]	0.999 (3+/5+) 0.958 (2+/6+)	$T_N = 12$ [39]		
$\text{Sr}_2\text{MnReO}_6$	$Fm\bar{3}m$, $a = 8.00$ [40]	0.997 (3+/5+) 0.949 (2+/6+)	$T_C = 120$ [40]		-10 [40] (100 K)
$\text{Ba}_2\text{MnReO}_6$	$Fm\bar{3}m$, $a = 8.18$ [40]	1.057 (3+/5+) 1.006 (2+/6+)	$T_C = 120$ [40]		+14 [40] (80 K)
Ca_2MnWO_6	$P2_1/n$, $a = 5.46$, $b = 5.65$ $c = 7.80$, $\beta = 90.2^\circ$ [41]	0.936 (3+/5+) 0.904 (2+/6+)	$T_C = 45$ $T_N = 16$ [41]		
Sr_2MnWO_6	$P4_2/n$, $a = 8.012$, $c = 8.01$ [42]	0.990 (3+/5+) 0.956 (2+/6+)	$T_C = 40$ $T_N = 13$ [42]		
Ba_2MnWO_6	$Fm\bar{3}m$, $a = 8.20$ [43]	1.049 (3+/5+) 1.014 (2+/6+)	$T_C = 45$ $T_N = 10$ [43]		
$\text{Ca}_2\text{FeMoO}_6$	$P2_1/n$, $a = 5.41$, $b = 5.52$, $c = 7.71$, $\beta = 90.0^\circ$ [31]	0.946 (3+/5+)	$T_C = 365$ [31]	3.51 [31]	-29 [44]
$\text{Sr}_2\text{FeMoO}_6$	$I4/mmm$, $a = 5.58$, $c = 7.89$ [20]	1.000 (3+/5+)	$T_C = 420$ [20]	3.7 [45]	-37 [5]
$\text{Ba}_2\text{FeMoO}_6$	$Fm\bar{3}m$, $a = 8.06$ [30]	1.060 (3+/5+)	$T_C = 367$ [30]	3.53 [31]	-25 [46] (8 kOe)
$\text{Ca}_2\text{FeReO}_6$	$P2_1/n$, $a = 5.40$, $b = 5.52$ $c = 7.68$, $\beta = 90.02^\circ$ [47]	0.943 (3+/5+)	$T_C = 540$ [48]	2.24 [49]	0 [47]
$\text{Sr}_2\text{FeReO}_6$	$Fm\bar{3}m$, $a = 7.89$ [47]	0.997 (3+/5+)	$T_C = 400$ [50]	2.7 [7]	-26 [47]
$\text{Ba}_2\text{FeReO}_6$	$Fm\bar{3}m$, $a = 8.06$ [47]	1.057 (3+/5+)	$T_C = 315$ [49]	3.04 [49]	-8 [47]
$\text{Ba}_3\text{Fe}_2\text{ReO}_9$	hexagonal, $a = 5.03$, $c = 14.10$ [38]				
Sr_2FeWO_6	$P2_1/n$, $a = 5.65$, $b = 5.61$ $c = 7.94$, $\beta = 89.99^\circ$ [51]	0.969 (2+/6+)	$T_N = 40$ [52]		
Ba_2FeWO_6	$I4m$, $a = 5.75$, $c = 8.13$ [51]	1.028 (2+/6+)	$T_N \approx 20$ [51]		

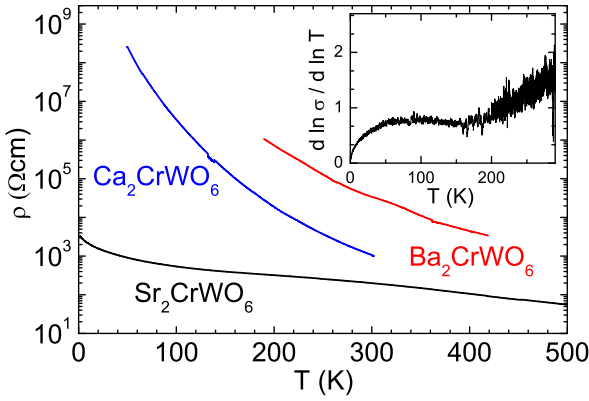


Figure 2: Resistivity vs temperature for the double perovskites $A_2\text{CrWO}_6$ with $A = \text{Sr}, \text{Ba}, \text{Ca}$. The inset shows $d \ln \sigma / d \ln T$ versus T (K) for the Sr_2CrWO_6 sample.

toresistance, $MR = [R(H) - R(0)]/R(0)$, of up to -41% at 5 K. At room temperature, this effect is reduced to a few percent. The large grain boundary MR effect at low temperatures indicates that Sr_2CrWO_6 has a large spin polarization of the charge carries and due to its high Curie temperature may be an interesting candidate for magnetoelectronic devices operating room-temperature.

C. Magnetic Properties

In Fig. 3 we plot the Curie temperature T_C , the saturation magnetization M_{sat} , and the ionic radii versus the tolerance factor for the series $A_2\text{CrWO}_6$. It is evident that the Curie temperature is largest for Sr_2CrWO_6 ($T_C = 458$ K), whereas it is suppressed strongly for Ca_2CrWO_6 ($T_C = 161$ K). We attribute this fact to the small ionic radius of Ca^{2+} , which results in $f \leq 1$ and, in turn, in a distorted perovskite structure. This results in a reduction of the effective hopping interactions between Cr 3d and W 5d states, leading to a reduced spin splitting of the conduction band [15]. This naturally reduces the magnetic coupling strength and hence the T_C .

The saturation magnetization M_{sat} is known to depend strongly on the amount δ of antisites, with $\delta = 0$ for no antisites and $\delta = 0.5$ for 50% antisites or complete disorder. By simply assuming the presence of antiferromagnetically coupled Cr and W sublattices, a maximum saturation magnetization of $2\mu_B/\text{f.u.}$ is expected for $\delta = 0$, which is decreasing to zero for $\delta = 0.5$. That is, this assumption leads to [45]

$$M_{\text{sat}}(\delta) = (1 - 2\delta) \cdot m(\text{Cr}^{3+}) - (1 - 2\delta) \cdot m(\text{W}^{5+}) , \quad (1)$$

where M_{sat} is the saturation magnetization in units of $\mu_B/\text{f.u.}$; $m(\text{Cr}^{3+})$ and $m(\text{W}^{5+})$ are the magnetic moments of the Cr^{3+} and W^{5+} ions in units of μ_B , respectively. Comparing the experimental data to this simple model prediction leads to a surprisingly good agreement for Sr_2CrWO_6 . The measured value of $M_{\text{sat}} =$

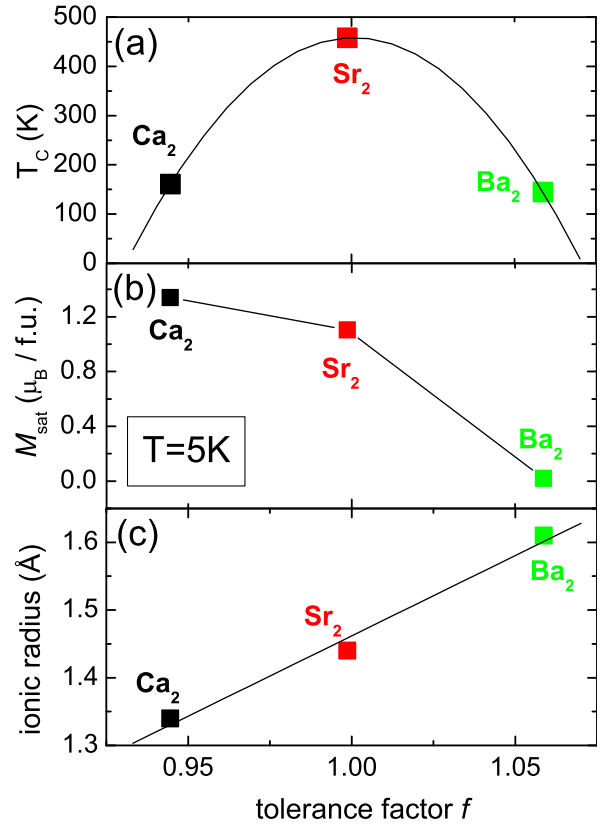


Figure 3: (a) Curie temperature, (b) saturation magnetization at 5 K and an applied field of 7 T, and (c) ionic radii for the series $A_2\text{CrWO}_6$ with $A = \text{Sr}, \text{Ba}, \text{Ca}$ plotted versus the tolerance factor f .

$1.11 \mu_B/\text{f.u.}$ is very close to the value of $1.08 \mu_B/\text{f.u.}$ expected from eq.(1) for $\delta = 0.23$. Fig. 3b also shows that the saturation magnetization of Ca_2CrWO_6 is larger than for Sr_2CrWO_6 despite the much lower Curie temperature of the latter. The obvious reason for that is the lower amount of antisites in Ca_2CrWO_6 . From the measured value of $\delta = 0.13$ we expect $M_{\text{sat}} = 1.48 \mu_B/\text{f.u.}$ for Ca_2CrWO_6 which is slightly larger than the measured value of $M_{\text{sat}} = 1.34 \mu_B/\text{f.u.}$. The reason for the observation that the experimental M_{sat} value is below the one predicted by eq.(1) most likely is the distorted crystal structure of Ca_2CrWO_6 .

The magnetic properties of the Ba_2CrWO_6 compound are completely different from those of Sr_2CrWO_6 and Ca_2CrWO_6 . Here, the large ionic radius of Ba^{2+} enlarges f well above unity. This causes a structural phase transition towards a hexagonal structure, where the ferromagnetic interaction is strongly suppressed. Therefore, not only T_C is strongly suppressed ($T_C = 145$ K, in contrast to $T_C = 458$ K for Sr_2CrWO_6), but also the saturation magnetization ($\sim 0.02 \mu_B/\text{f.u.}$) is close to zero. This clearly indicates the strong effect of the structural phase transition on the magnetic interaction. We note that we can exclude the possibility that the very small M_{sat} value

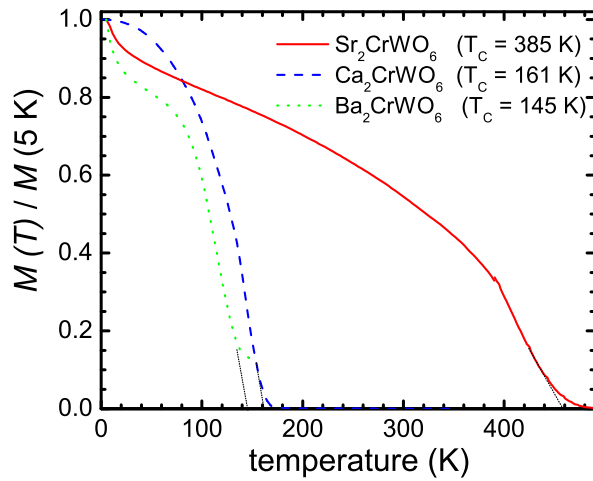


Figure 4: Normalized magnetization versus temperature for the series $A_2\text{CrWO}_6$ with $A = \text{Sr, Ba, Ca}$. The measurements were made field cooled in an applied field of $H = 100$ Oe. The black lines represent are extrapolations of the measured data for the determination of T_C . Due to the small M_{sat} of the Ba_2CrWO_6 compound, the zero line is shifted due to a small residual paramagnetic moment in the applied field.

is due to strong disorder. Evidently, there should be almost complete disorder to suppress M_{sat} close to zero. However, in the Ba_2CrWO_6 compound the two different B sites establish a certain amount of order, since almost all W ions occupy the B_2 site. Whether the observed behavior is related to a canted antiferromagnetic phase or simply to the presence of minority phases has to be clarified.

Fig. 4 shows that the magnetic interactions for all three compounds $A_2\text{CrWO}_6$ is ferromagnetic. However, the strongly reduced saturation magnetization of Ba_2CrWO_6 and the upturn in magnetization vs. temperature curve at low temperatures indicates that ferromagnetic interactions are small and that there may be paramagnetic regions in the sample. The substitution of Sr by Ca evidently results in a strong reduction of T_C , however, the Ca_2CrWO_6 samples are still clearly ferromagnetic. Again, the important point is that only the compound with $f \simeq 1$ has optimum magnetic properties with respect to applications in magnetoelectronics.

We also have performed measurements of the coercive field H_c . At low temperature we obtained $H_c \simeq 450$ Oe for the Sr_2CrWO_6 compound and $H_c \simeq 6000$ Oe for the Ca_2CrWO_6 compound. Furthermore, for the Sr_2CrWO_6 the coercive field was found to depend on the preparation conditions. For example, lowering the final firing temperature from 1550°C to 1300°C was found to increase H_c from 450 to 1200 Oe. In agreement with the findings for the doped manganites [35], the coercive field increases with decreasing f . This observation can be easily understood, since the induced structural distortions can effectively act as pinning centers for domain wall movement. In those cases where a large remanent magnetiza-

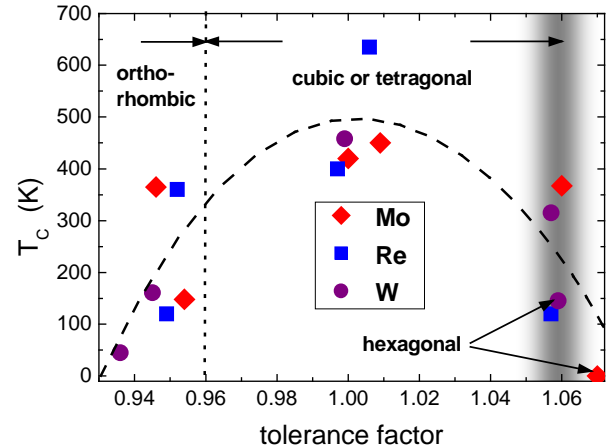


Figure 5: Curie temperature of the different double perovskite materials listed in Table II plotted versus their tolerance factor. Re-compounds: squares, W-compounds: circles, Mo-compounds: diamonds. The broken line only serves as a guide to the eyes.

tion and/or coercive field are important for applications, the use of double perovskites with reduced values of f obtained by suitable substitution on the A -site may be desirable.

Comparing our results for the series $A_2\text{CrWO}_6$ with $A = \text{Sr, Ba, Ca}$ to other double perovskite compounds summarized in Table II, it is evident that the suppression of T_C as a function of the deviation of the tolerance factor from its ideal value of $f = 1$ is a general trend: It is only weak for the series $A_2\text{FeMoO}_6$ with $A = \text{Sr, Ba, Ca}$, where T_C varies between 310 K and 420 K [30, 31, 32, 33, 53]. However, it is also strong for the series $A_2\text{CrReO}_6$ with $T_C = 635$ K for $\text{Sr}_2\text{CrReO}_6$ and $T_C = 360$ K for $\text{Ca}_2\text{CrReO}_6$ [2]. In general, a high Curie temperature can only be realized in double perovskites of the composition $A_2\text{BB}'\text{O}_6$ having a tolerance factor close to unity. This is realized in the different systems for $A_2 = \text{Sr}_2$. For f well below unity, the Curie temperature is drastically reduced in agreement with what is found for the doped manganites [34]. For the double perovskites, the system $(\text{Sr}_{1-y}\text{Ca}_y)_2\text{FeReO}_6$ is an exception of the general rule [50]: Here, the $\text{Ca}_2\text{FeReO}_6$ compound has the highest T_C , although the tolerance factor decreases continuously from $f = 0.997$ for $\text{Sr}_2\text{FeReO}_6$ to $f = 0.943$ for $\text{Ca}_2\text{FeReO}_6$ on substituting Sr by Ca. We note, however, that $\text{Ca}_2\text{FeReO}_6$ is a unique material as it is a ferromagnetic insulator and that there may be an other mechanism causing the high ordering temperature [49].

In Fig. 5 we have plotted the Curie temperatures of the double perovskite materials listed in Table II versus their tolerance factor omitting the ferromagnetic insulator $\text{Ca}_2\text{FeReO}_6$. Despite the significant spread of data that may be partially caused by different sample quality, it is evident that a maximum Curie temperature is obtained for the systems having a tolerance factor of $f \simeq 1$.

These systems have a cubic/tetragonal symmetry. As shown in Fig. 5, for $f < 1$ there is a transition to orthorhombic structures for $f \sim 0.96$, whereas for $f > 1$ there is a transition to a hexagonal structure at $f \sim 1.06$. However, according to data from literature this transition seems to be smeared out as indicated by the shaded area.

D. Underlying Physics

We briefly summarize the measured structural, transport and magnetic properties and discuss the underlying physics. Recently, Sarma *et al.* proposed an interesting model explaining the origin of the strong antiferromagnetic coupling between Fe and Mo in $\text{Sr}_2\text{FeMoO}_6$ in terms of an strong effective exchange enhancement at the Mo site due to a Fe 3d-Mo 4d hybridization [15]. Kanamori and Terakura extended this idea to explain ferromagnetism in many other systems, where nonmagnetic elements positioned between high-spin 3d elements contribute to the stabilization of ferromagnetic coupling between the 3d elements [16]. The essence of this model is summarized in Fig. 6a for the case of $\text{Sr}_2\text{FeMoO}_6$. Without any hopping interactions, the Fe^{3+} 3d⁵ configuration has a large exchange splitting of the 3d level in the spin-up and spin-down states and there is also a crystal field splitting Δ into the t_{2g} and the e_g states (see Fig. 6a). The exchange splitting of the Mo^{5+} 4d¹ configuration (better the Mo-4d-O-2p hybridized states) is vanishingly small, however, there is a large crystal field splitting (the e_g states are several eV above the t_{2g} states and not shown in Fig. 6a). The interesting physics occurs on switching on hopping interactions, which result in a finite coupling between states of the same symmetry and spin. The hopping interaction not only leads to an admixture of the Fe 3d to the Mo 4d states, but more importantly to a shift of the bare energy levels. As shown in Fig. 6a, the delocalized Mo 4d spin-up states are pushed up, whereas the Mo 4d spin-down states are pushed down. This causes a finite spin polarization at the Fermi level (actually 100% in Fig. 6a) resulting from the hopping interactions. This kinetic energy driven mechanism leads to an antiferromagnetic coupling between the delocalized Mo 4d and the localized Fe 3d electrons, since the energy is lowered by populating the Mo 4d spin-down band [15]. The magnitude of the spin polarization derived from this mechanism obviously is governed by the hopping strength and the charge transfer energy between the localized and the delocalized states [16].

The question now arises, whether the above model also applies for the A_2CrWO_6 compounds. The key concept of the model is the energy gain contributed by the spin polarization of the nonmagnetic element (now W) induced by the hybridization with the magnetic transition metal (now Cr). It has been pointed out by Sarma [15] that the underlying mechanism will always be operative, whenever the conduction band is placed within the energy gap formed by the large exchange splitting of the

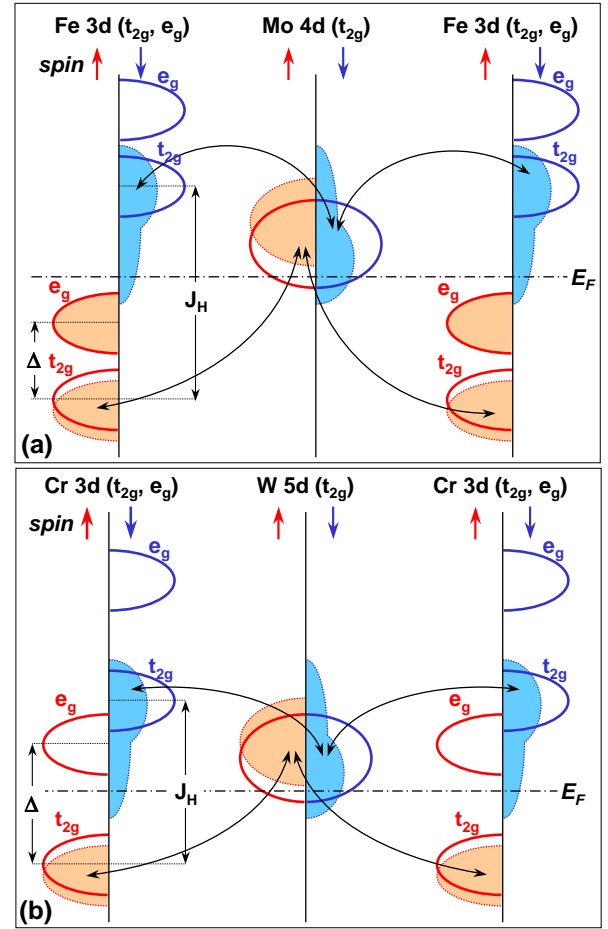


Figure 6: Sketch of the band structure for the illustration of the mechanism stabilizing the ferromagnetic state in the double perovskites. (a) shows the situation for A_2FeMoO_6 . Here, the Fermi energy lies between the exchange split 3d spin-up and -down states. In (b) we show the situation for A_2CrWO_6 . Here, the Fermi level lies in the crystal-field split Cr 3d spin-up band between the t_{2g} and the e_g levels. The solid lines mark the bands without hybridization, whereas the shaded areas denote the bands with hybridization. The arrows connect the hybridizing bands. The hybridization between the e_g level has been neglected.

localized electrons at the transition metal site. As shown in Fig. 6b, this is also the case for the A_2CrWO_6 compounds: the W 5d band resides in between the exchange split Cr 3d (t_{2g}) spin-up and spin-down bands. The schematic band structure of Fig. 6b has been confirmed by band structure calculations presented below. The only difference between the system A_2CrWO_6 and the systems A_2FeMoO_6 or A_2FeReO_6 is the fact that in the former the majority spin band is only partially full. For Cr^{3+} , ($3d^3, S = 3/2$) only the Cr t_{2g} levels are occupied. In contrast, for Fe^{3+} ($3d^5, S = 5/2$) both the Fe t_{2g} and Fe e_g levels are occupied, that is, the majority spin band is completely filled. Band structure calculations show that the crystal field splitting in the Cr compounds (~ 2 eV) is slightly larger than in the Fe compounds [58]. On the

other hand, the exchange splitting in the Cr 3d bands is somewhat smaller than for the Fe 3d bands due to the valence configuration Cr 3d³ with less electrons and weaker Hund's coupling. Taking these facts into account we have to split up the Cr 3d spin-up and spin-down band into two separate 3d (t_{2g}) and 3d (e_g) bands with the Fermi level lying in the gap between the bands as shown in Fig. 6b. Indeed band structure calculations (see below) show that the Cr 3d (e_g) spin-up band is about 0.5 eV above the Fermi level. However, the above mechanism still works as long as the W 5d (t_{2g}) band is placed within the energy gap between the Cr 3d (t_{2g}) spin-up and the Cr 3d (t_{2g}) spin-down band. Then, again the W 5d (t_{2g}) levels would hybridize with the Cr 3d (t_{2g}) levels resulting in a negative spin polarization of the nonmagnetic element W 5d (t_{2g}) and a stabilization of ferromagnetism and half-metallic behavior. We note that no hybridization takes place between the Cr 3d (e_g) spin-up band and the W 5d (t_{2g}) spin-up band due to the different symmetry of these levels. Therefore, the exact position of the Cr 3d (e_g) spin-up band is not relevant. We also note that due to the large crystal field splitting for the W 5d band, the W 3d (e_g) band is several eV above the W 3d (t_{2g}) band and not shown in Fig. 6b. Summarizing our discussion we can state that the essential physical mechanism leading to ferromagnetism is very similar for the $A_2\text{CrWO}_6$ and the $A_2\text{FeMoO}_6$ compounds. Comparing Fig. 6a and b we see that the only difference is an upward shift of the 3d bands for the $A_2\text{CrWO}_6$ compounds.

We now discuss the experimental results in context with the models discussed above. We first discuss the strong dependence of T_C on the tolerance factor, which in turn is intimately related to the bond angles. It is well known that in perovskite type transition metal oxides in general the increase of the B-O bond length and the deviation of the B-O-B bond angle from 180° has the effect of a reducing the hybridization matrix element t . This is caused by the reduction of the overlap of the oxygen 2p and transition-metal d states [54], which in turn results in a reduction of the bare electron bandwidth W . Since the weakening of the hybridization causes a reduction of the energy gain stabilizing ferromagnetism, we expect a significant decrease of T_C with increasing deviation of the tolerance factor from $f = 1$, or equivalently with an increasing deviation of the B-O-B bond angle from 180°. This is in good qualitative agreement with our results on the $A_2\text{CrWO}_6$ compound (see Fig. 3a) and the collected data plotted in Fig. 5. Theoretical models providing a quantitative explanation have still to be developed.

It is known that for a 180° bond angle, t decreases with increasing bond length $d_{\text{B}-\text{O}}$ roughly as $t \propto 1/d_{\text{B}-\text{O}}^{3.5}$. Therefore, the effective hopping amplitude between the transition metal ions B has an even stronger dependence on $d_{\text{B}-\text{O}}$. Hence, a significant increase of t and, in turn, T_C is expected with a reduction of the bond length. Applying this consideration to the investigated series $A_2\text{CrWO}_6$ we would expect the largest T_C for the Ca_2CrWO_6 compound due to its smallest cell volume

and, hence, shortest bond length. However, experimentally the largest T_C was found for Sr_2CrWO_6 . This is caused by the fact that t not only depends on the bond length but also strongly on the bond angle. For the cubic double perovskite Sr_2CrWO_6 with $f \simeq 1$ the bond angle has the ideal value of 180°, whereas for the distorted double perovskite Ca_2CrWO_6 with $f < 1$ the bond angle significantly deviates from this ideal value. For the double perovskites lattice effects come into play also for large tolerance factors $f \gtrsim 1.06$, where in the hexagonal structure the formation of dimers suppresses strongly ferromagnetism and enhances antiferromagnetic interactions. Furthermore, the magnetic interactions are also weakened due to the increased distance (bond length) between the magnetic ions. We finally would like to mention that in a recent work on $A_2\text{FeMoO}_6$, a linear correlation, $T_C \propto W$, between T_C and the bare one-electron bandwidth $W \propto t$ has been found by Ritter *et al.* [31].

Summarizing our discussion we can state that our findings for the series $A_2\text{CrWO}_6$ can be extended to the double perovskites in general. The data summarized in Table II and Fig. 5 clearly indicated that for most double perovskites a maximum T_C is obtained for a tolerance factor of $f \simeq 1$ corresponding to an about cubic perovskite structure with a bond angle close to 180°. This optimum situation in most cases is realized in the $\text{Sr}_2\text{BB}'\text{O}_6$ compounds. The requirement $f \simeq 1$ for optimum T_C in the double perovskite is different for the doped manganites. Here, a maximum T_C is achieved for compounds with $f \lesssim 0.95$, that is, for a significantly distorted perovskite structure. Hwang *et al.* [34] have shown that the highest T_C in doped manganites is obtained for $f \simeq 0.93$ (in a more precise analysis by Zhou *et al.* [35] slightly larger values for f have been derived based on a coordination number of 9). For a tolerance factor below the optimum value, a dramatic decrease of T_C has been found. Whether or not the differences between the manganites and the double perovskites are related to the different mechanism stabilizing ferromagnetism in these compounds has to be clarified. We note, however, that the different behavior of the manganites and the double perovskites is likely to be related to different mechanisms. In manganites the polarization of the conduction band is driven by the Hund's coupling (intra atomic) between the t_{2g} and the e_g states, which is not sensitive to the details of the band structure. In contrast, in the double perovskites the spin polarization of the conduction band is itself dependent on the band structure and therefore is more intimately linked to it.

IV. ELECTRON DOPING IN Sr_2CrWO_6

The effect of carrier (electron) doping in Sr_2CrWO_6 was studied in a series of $\text{Sr}_{2-x}\text{La}_x\text{CrWO}_6$ samples with $x = 0, 0.1, 0.3$ and 0.5 . In our experiments trivalent La^{3+} is chosen to replace the Sr^{2+} ions because the ionic radius of La^{3+} ($r_{\text{La}^{3+}} = 1.36 \text{ \AA}$) is similar to that of Sr^{2+}

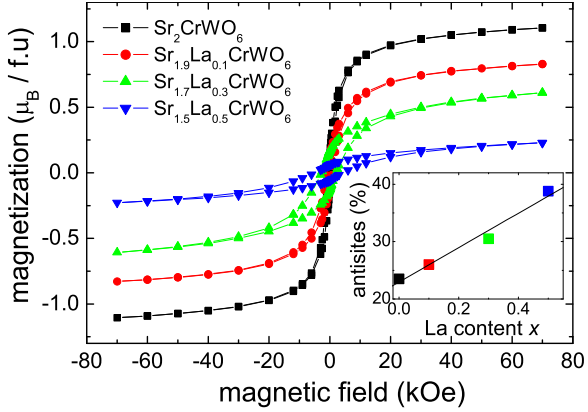


Figure 7: Magnetization vs. applied magnetic field at $T = 5$ K for the series $\text{Sr}_{2-x}\text{La}_x\text{CrWO}_6$ with $x = 0, 0.1, 0.3$ and 0.5 . The inset shows the amount of antisites determined a Rietveld refinement of the x-ray data.

($r_{\text{Sr}^{2+}} = 1.44 \text{ \AA}$). As a result, there are only a small variations of the lattice parameters and the tolerance factor f on changing the doping level from $x = 0$ to $x = 0.5$. X-ray analysis showed that the lattice parameter slightly decreases from 7.818 \AA ($x = 0$) to 7.804 \AA ($x = 0.5$) as expected since the ionic radius of La^{3+} is smaller than that of Sr^{2+} . However, the crystal structure of all samples remained cubic. This means that the structural changes are small on varying the doping level. In this way the effect of doping can be studied without being strongly influenced by structural effects.

In Fig. 7 the magnetization curves of the series $\text{Sr}_{2-x}\text{La}_x\text{CrWO}_6$ are shown for $T = 5$ K. All samples of this series have been fired between 1530 and 1550°C in reducing atmosphere. For the undoped sample this results in a smaller Curie temperature of about 390 K as compared to about 460 K for the samples fired at 1300°C . The reason for that most likely is a slightly smaller oxygen content in the sample fired at a higher temperature. Since a reduced oxygen content corresponds to an effective electron doping, for the doping series we compare only samples prepared under identical conditions. We find that the saturation magnetization M_{sat} decreases from $1.11 \mu_B/\text{f.u.}$ for $x = 0$ to $0.23 \mu_B/\text{f.u.}$ for $x = 0.5$. As shown in the inset of Fig. 7, with increasing doping level also the amount of antisites is increasing. At present, we only have a plausible explanation for the observed increase of the amount of antisites with increasing doping level, which so far could not be unambiguously proven. However, since La doping is expected to result in a reduction of the differences in the valence states of Cr and W, it evidently results in a reduction of the differences in the ionic radii of Cr and W ($r_{\text{Cr}^{2+}}/r_{\text{W}^{6+}} = 0.73/0.63$ and $r_{\text{Cr}^{3+}}/r_{\text{W}^{5+}} = 0.615/0.62$). Therefore, increasing the doping level results in more similar ionic radii of Cr and W paving the way for the creation of Cr/W antisites. Since the substitution of Sr^{2+} by La^{3+} results both in electron doping and an increase

of antisites, it is not possible to unambiguously attribute the measured decrease in M_{sat} to either the increasing doping level or the increase of antisites alone. As will be discussed in the following, for the series $\text{Sr}_{2-x}\text{La}_x\text{CrWO}_6$ the measured reduction of M_{sat} most likely is caused by both electron doping and disorder.

We first discuss the expected reduction of M_{sat} due to the increasing amount of antisites. We note that several authors have found a reduction of M_{sat} following the increase of antisites [4, 45]. This behavior is consistent with simple Monte Carlo simulation studies [55]. However, also more complicated models [15, 16, 17] predict a reduction of M_{sat} with increasing amount of antisites due to charge transfer effects [57]. In a first approach we can analyze our data using eq.(1). With the measured δ values for the amount of antisites we can calculate $M_{\text{sat}}(\delta)$. We find that the calculated M_{sat} values are significantly larger than the measured ones. This suggests that the observed reduction of the saturation magnetization cannot be explained by the increasing amount of antisites alone (at least within the simple model yielding eq.(1)). However, we also have to keep in mind that electron doping itself contributes to the reduction of M_{sat} . According to the illustration given in Fig. 6a it is evident that electron doping in the A_2FeMoO_6 system increases the spin-down magnetic moment at the Mo site, indicating that the electrons are filled into the Mo $4d_{\downarrow}$ band and thereby reduce M_{sat} [14]. According to Fig. 6b, the same mechanism holds for the $\text{Sr}_{2-x}\text{La}_x\text{CrWO}_6$ system. That is, our results suggest that the observed reduction of the saturation magnetization with increasing La^{3+} substitution is caused both by an increase of the amount of antisites and an increase of the number of conduction electrons.

Summarizing our discussion of the saturation magnetization we would like to emphasize that a variation of the doping level in most cases is correlated with a variation of the amount of disorder, since doping contributes to a reduction of the difference of the valence states of Cr and W (Fe and Mo) what in turn results in an increasing amount of antisites [56]. Unfortunately, due to this fact the experimental situation is not completely clear. While in [4] for $\text{Sr}_2\text{FeMoO}_6$ and also in our study for Sr_2CrWO_6 La doping is clearly correlated with higher disorder, in [14] the amount of antisites seems to be constant in $\text{Sr}_{2-x}\text{La}_x\text{FeMoO}_6$ for almost the whole doping series from $x = 0$ to $x = 0.3$. For the system Sr_2CrWO_6 , the suppression of M_{sat} is stronger than for the system $\text{Sr}_2\text{FeMoO}_6$, probably due to the fact that the Cr and W ions are easier to disorder because of their similar ionic radii. We finally note that in general both increasing doping and disorder can destroy the underlying half-metallic ferromagnetic state in double perovskites, thereby significantly populating/depopulating the different spin channels leading to a sharp decrease in M_{sat} [57].

We next discuss the influence of La doping on the Curie temperature. It is evident that an enhancement of T_C by doping would be of great importance for possible applications of the double perovskites in spintronic

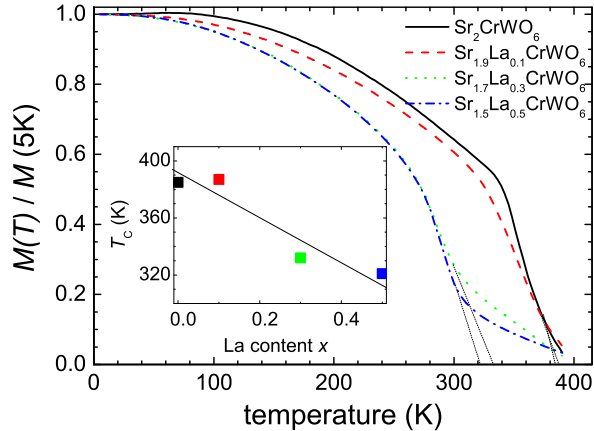


Figure 8: Normalized magnetization vs temperature for the series $\text{Sr}_{2-x}\text{La}_x\text{CrWO}_6$ with $x = 0, 0.1, 0.3$, and 0.5 . The measurements were made field cooled in $H = 100$ Oe. The inset shows the Curie temperature as a function of the La doping.

devices. However, both the experimental data on the variation of T_C with electron doping as well as the theoretical interpretation is controversial at present. In single crystals of $\text{Sr}_{2-x}\text{La}_x\text{FeMoO}_6$ Moritomo *et al.* have found that T_C does not change as a function of La doping $x \leq 0.3$ [14]. In contrast, Navarro *et al.* have reported a considerable increase of T_C of about 70 K in ceramic samples of $\text{Sr}_{2-x}\text{La}_x\text{FeMoO}_6$ investigating a wider doping range $0 \leq x \leq 1$ [4]. In our study on the system $\text{Sr}_{2-x}\text{La}_x\text{CrWO}_6$ we have found a reduction of T_C of about 80 K in the doping range $0 \leq x \leq 0.5$ as can be seen in Fig. 8. We note that part of the experimental discrepancies may be related to large error bars in the determination of T_C . In particular, great care has to be taken over the determination of T_C , since the transition from zero magnetization to finite magnetization is smeared out considerably due to finite applied magnetic fields and parasitic phases. It is evident from Fig. 8 that in all our samples there are minor phases with optimum T_C close to about 400 K. However, it is also evident that La doping reduces T_C of the major part of the sample. That is, different experimental results on T_C may be in part related to different ways of measuring and analyzing the data.

From the theoretical point of view one expects both an increase and decrease of T_C with increasing doping. On the one hand, within the model presented in [15, 16, 17] T_C is expected to be rather reduced than enhanced by electron doping due to the fact that the possible energy gain by shifting electrons from spin-up band into the spin-down band is reduced [19]. This, in turn, reduces the stability of the ferromagnetic phase in agreement with our results. However, the role of the increasing amount of antisites with increasing doping still has to be clarified. On the other hand, in a double exchange model the increase of the number of conduction electrons promoted

by La doping is expected to enhance the double exchange interaction leading to an increase of T_C . Within this model the ferromagnetic interaction arises from the double exchange interaction between the localized moments on Cr^{3+} sites ($3d^3$, $S = 3/2$) mediated by itinerant electron provided by the W^{5+} ions ($5d^1$, $S = 1/2$). According to the band structure calculation presented below, the $\text{Cr} t_{2g}$ spin-up subband is completely filled and it is the electron in the t_{2g} spin-down subband of Cr and W which mediates the double exchange interaction. In general, an increasing number of electrons in the spin-down subband is expected to strengthen the double exchange interaction leading to an increase of T_C in conflict with our experimental findings. That is, the observed decrease of T_C with increasing doping level seems to support the model presented in [15, 16, 17] (see also Fig. 6). However, we have to take into account that by La doping besides the number of electrons we also increase the amount of disorder. The latter may weaken the double exchange interaction sufficiently to result in an effective decrease of T_C also within a double exchange based model. Further work is required to clarify this in more detail.

V. BAND STRUCTURE CALCULATIONS AND OPTICAL MEASUREMENTS ON Sr_2CrWO_6

A. Band Structure Calculations

The half-metallicity of ferromagnetic materials is one of the important ingredients required for applications. In order to obtain a conclusive picture regarding the spin polarization at the Fermi level it is important to compare band structure calculations with experimental results. Here, we compare the results of band structure calculations based on *ab initio* methods to experimental results on the optical reflectivity and transmissivity.

In Fig. 9 the density of states of Sr_2CrWO_6 is plotted versus energy. The band structure has been calculated [15, 57] within the linear muffin-tin orbital (LMTO) method using the atomic sphere approximation (ASA). A detailed discussion of this method can be found elsewhere [59, 60]. As a key result of the calculation we obtain a gap of about 0.7 eV in the spin-up band around the Fermi level (compare also Fig. 6b). This gap corresponds to gap between the crystal field split Cr $3d$ (t_{2g}) and Cr $3d$ (e_g) subband. On the other hand, the spin-down states are available at the Fermi-level. The broad band corresponds to the hybridized Cr $3d$ (t_{2g}) and W $5d$ (t_{2g}) levels. That is, according to the band structure calculation we expect a half-metallic behavior for the double perovskite Sr_2CrWO_6 . A similar result but with slightly larger band gaps has been reported recently by Jeng *et al.* [58]. The result of the band structure calculation is in agreement with the model assumptions made above. The Cr $3d$ (t_{2g}) spin-up subband is completely filled and there is a gap to the Cr $3d$ (e_g) spin-up subband lying about 0.5 eV above the Fermi level. The W $5d$ (t_{2g}) spin-

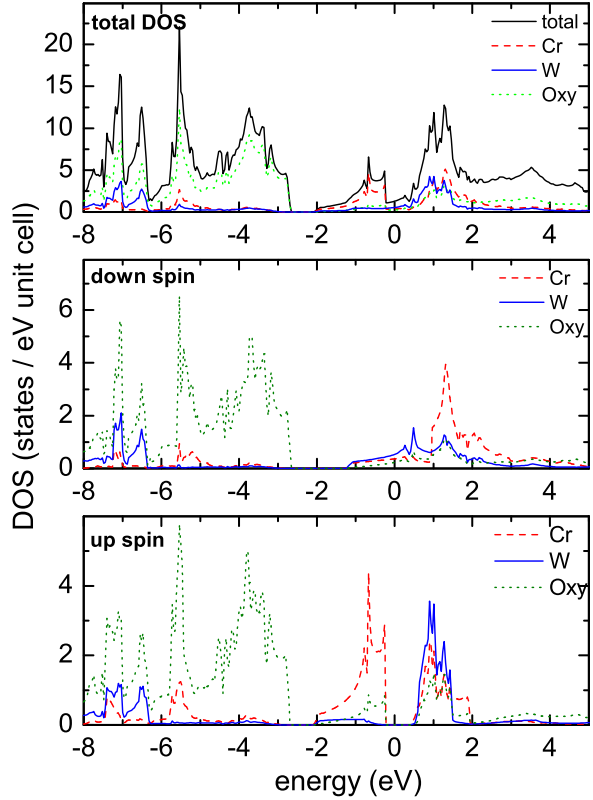


Figure 9: Density of states obtained from *ab initio* band structure calculations for Sr_2CrWO_6 plotted as a function of energy with $E_{\text{Fermi}} = 0$.

up band also is mainly above the Fermi level. The hybridized Cr 3d (t_{2g}) spin-down states and the W 5d (t_{2g}) spin-down states form a broad spin-down band with the Fermi level lying in this band. This is fully consistent with the model presented in Fig. 6. Furthermore, the band structure calculation shows that La doping is expected to add electrons in the spin-down band.

B. Optical Measurements

In order to verify the band structure calculations experimentally, we have performed optical reflection and transmission measurements of Sr_2CrWO_6 thin films with photon energies from 0.38 eV to 7 eV. The SrTiO_3 substrates, on which the epitaxial quality of the films is high (see Fig. 1), are unfortunately transparent only in the range of photon energies of 0.20-3.2 eV. Therefore, we have also investigated strained epitaxial Sr_2CrWO_6 films on LaAlO_3 substrates, which are transparent from 0.17 to 5.5 eV, and polycrystalline Sr_2CrWO_6 films on MgAl_2O_4 substrates, which are transparent from 0.22-6.5 eV, however have a larger lattice mismatch to Sr_2CrWO_6 . On each substrate, films with thicknesses of $d = 30$, 80, and 320 nm were investigated. Almost identical optical absorption spectra were obtained for the epitaxial

films, suggesting that the observed optical features are indeed related to the Sr_2CrWO_6 films, as summarized in Fig. 10. The dominant optical features, which are an absorption shoulder around 1 eV, and a strong increase of the absorption above 4 eV, are also found for the polycrystalline samples grown on MgAl_2O_4 . The transmission T at 4.6 eV is around 0.1% for the films with $d = 320$ nm, and around 30% for the films with $d = 30$ nm. The error in the calculation of the absorption coefficient $\alpha = \ln[(1 - R)^2/T]/d$ with the reflection R comes mostly from uncertainties in R/T , which is sufficiently small for the 320 nm films at lower energies, and for the 30 nm films at higher energies. For the films with $d = 320$ nm, reflectivity oscillations with a period $p = 0.77 \pm 0.07$ eV were observed at photon energies of 1.5-3.5 eV, indicating a refractory index $n = hc/(2 d p) = 2.5 \pm 0.2$. This is consistent with the measured reflection data and $R = (n - 1)^2/(n + 2)^2 \approx 18 \pm 4\%$ in this energy range. As determined from Fourier transform infrared (FTIR) transmission measurements, the films remain transparent down to 0.2 eV, however, R is increasing significantly towards lower photon energies.

The optical measurements agree fairly well with the band structure calculations. The increase of the absorption coefficient of Sr_2CrWO_6 above 4 eV can most probably be attributed to a charge transfer transition between the p-like spin-up and -down oxygen bands at -3 eV below the Fermi-level into the oxygen/metal bands at $+1$ eV above the Fermi-level. The absorption shoulder around 1 eV coincides roughly with the energy gap at the Fermi level in the spin-up band, and is therefore probably caused by transitions from the Cr spin-up t_{2g} states below the Fermi-level into the oxygen/metal bands around $+1$ eV above the Fermi-level. Unfortunately, due to the substrate absorption below 0.2 eV, no optical information is available in the infrared region which would allow a more definitive statement with respect to the density of states at the Fermi level and the half-metallic character of Sr_2CrWO_6 . However, from the refractory index $n \approx 2.5$, one can estimate an optical conductivity of $\sigma_{\text{opt}} = \alpha n \epsilon_0 \approx 630 \Omega^{-1} \text{cm}^{-1}$ at 1 eV. Comparing this result with recent measurements of $\text{Sr}_2\text{CrReO}_6$ [2], one can classify Sr_2CrWO_6 as a (very) bad half metal. This is also in agreement with recent transport measurements [8]. We note, however, that the transport data may be ambiguous, since the conductivity of the Sr_2CrWO_6 thin film is comparable to that of the substrate. This is for example the case for SrTiO_3 substrates, which obtain a conductive surface layer at the reducing atmosphere of the thin film deposition process [24]. That is, more conclusive transport data are required to settle this issue.

Summary

We have performed a detailed analysis of the structural, transport, magnetic and optical properties of the double perovskite $A_2\text{CrWO}_6$ with $A = \text{Sr}, \text{Ba}, \text{Ca}$.

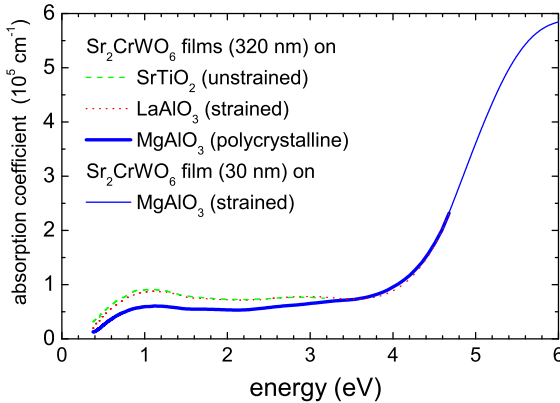


Figure 10: Optical absorption coefficients of Sr_2CrWO_6 thin films calculated from reflection and transmission measurements at room temperature. The films on SrTiO_3 (transparent in the range of 0.20–3.2 eV) and LaAlO_3 (0.17–5.5 eV) were epitaxial, and those on MgAl_2O_3 (0.22–6.5 eV) were polycrystalline. 30 nm thin films were used for quantitative measurements at high absorption coefficients above 4.6 eV.

In agreement with band structure calculations the double perovskite Sr_2CrWO_6 is a half-metal with a high Curie-temperature above 450 K. The measured saturation magnetization of $1.11 \mu_B/\text{f.u.}$ is well below the optimum value of $2 \mu_B/\text{f.u.}$ due to 23% of Cr/W antisites. The large amount of antisites most likely is caused by the similar ionic radii of the Cr^{3+} and W^{5+} ions resulting in a low threshold for the formation of antisites.

The substitution of Sr by Ba and Ca in the double perovskite system A_2CrWO_6 showed that the maximum Curie temperature is obtained for the compound with a

tolerance factor close to one. This is in agreement with a large variety of data reported in literature on other double perovskite systems $\text{A}_2\text{BB}'\text{O}_6$. The fact that the maximum T_C is obtained for a tolerance factor close to one differs from the behavior of the doped manganites where a maximum T_C was found for a tolerance factor of about 0.93. The observation that a tolerance factor $f \simeq 1$ yields the highest T_C has been explained within a model, where ferromagnetism is stabilized by the energy gain contributed by the negative spin polarization on the nonmagnetic W-site due to hybridization of the Cr 3d (t_{2g}) and the W 5d (t_{2g}) states. This hybridization is weakened by bond angles deviating from 180° or equivalently a tolerance factor deviating from unity.

Electron doping of Sr_2CrWO_6 by partial substitution of Sr^{2+} by La^{3+} was found to decrease both the Curie temperature and the saturation magnetization. The decrease in the saturation magnetization was found to be caused both by an increase in the amount of antisites and by increasing band filling. Although the decrease of T_C with increasing doping can be explained qualitatively within the same model, it seems to be in conflict with double exchange type models predicting an increase of T_C with increasing band filling. However, an unambiguous conclusion cannot be drawn at present. The reason for that is the fact that on increasing the doping level one also obtains an increasing amount of disorder. In order to clarify this issue it is required to study systems allowing for the variation of the doping level without changing disorder.

This work was supported by the Deutsche Forschungsgemeinschaft and the Bundesministerium für Bildung und Forschung (project 13N8279). The authors acknowledge fruitful discussions with M. S. Ramachandra Rao.

[1] K.-I. Kobayashi, T. Kimura, H. Sawada, K. Terakura, and Y. Tokura, *Nature* **395**, 677 (1998).

[2] H. Kato, T. Okuda, Y. Okimoto, Y. Tomioka, Y. Takenoya, A. Ohkubo, M. Kawasaki, and Y. Tokura, *Appl. Phys. Lett.* **81**, 328 (2002).

[3] S. A. Wolf, D. D. Awschalom, R. A. Buhrman, J. M. Daughton, S. von Molnar, M. L. Roukes, A. Y. Chtchelkanova, D. M. Treger, *Science* **294**, 1488 (2001).

[4] J. Navarro, C. Frontera, Ll. Balcells, B. Martínez, and J. Fontcuberta, *Phys. Rev. B* **64**, 092411 (2001).

[5] D. D. Sarma, E. V. Sampathkumaran, Sugata Ray, R. Nagarajan, S. Majumdar, A. Kumar, G. Nalini, and T. N. Guru Row, *Sol. State Comm.* **114**, 465 (2000).

[6] M. García-Hernández, J. L. Martínez, M. J. Martínez-Lope, M. T. Casais, and J. A. Alonso, *Phys. Rev. Lett.* **86**, 2443 (2001).

[7] K.-I. Kobayashi, T. Kimura, Y. Tomioka, H. Sawada, K. Terakura, and Y. Tokura, *Phys. Rev. B* **59**, 11159 (1999).

[8] J. B. Philipp, D. Reisinger, M. Schonecke, A. Marx, A. Erb, L. Alff, R. Gross, and J. Klein, *Appl. Phys. Lett.* **79**, 3654 (2002).

[9] D. Serrate, J. M. De Teresa, J. Blasco, M. R. Ibarra, L. Morellón, and C. Ritter, *Appl. Phys. Lett.* **80**, 4573 (2002).

[10] F. Galasso, F. C. Douglas, R. Kasper, *J. Chem. Phys.* **44**, 1672 (1966).

[11] F. K. Patterson, C. W. Moeller, R. Wald, *Inorg. Chem.* **2**, 196 (1963).

[12] J. Longo, R. Wald, *J. Am. Chem. Soc.* **83**, 2816 (1961).

[13] Y. Moritomo, Sh. Xu, A. Machida, T. Akimoto, E. Nishibori, M. Takata, and M. Sakata, *Phys. Rev. B* **61**, R7827 (2000).

[14] Y. Moritomo, Sh. Xu, T. Akimoto, A. Machida, N. Hamada, K. Ohoyama, E. Nishibori, M. Takata, and M. Sakata, *Phys. Rev. B* **62**, 14224 (2000).

[15] D. D. Sarma, P. Mahadevan, T. Saha-Dasgupta, Sugata Ray, and A. Kumar, *Phys. Rev. Lett.* **85**, 2549 (2000); see also *Curr. Opinion in Solid State Mat. Sci.* **5**, 261 (2001).

[16] J. Kanamori and K. Terakura, *J. Phys. Soc. Jpn.* **70**, 1433 (2001).

[17] Z. Fang, K. Terakura, and J. Kanamori, *Phys. Rev. B* **63**, R180407 (2001).

[18] M. Tovar, M. T. Causa, and A. Butera, J. Navarro, B. Martinez, and J. Fontcuberta, M. C. G. Passeggi, Phys. Rev. B **66**, 024409 (2002).

[19] K. Phillips, A. Chattopadhyay, and A. J. Millis, Phys. Rev. B **67**, 125119 (2003).

[20] Y. Tomioka, T. Okuda, Y. Okimoto, R. Kumai, K.-I. Kobayashi, and Y. Tokura, Phys. Rev. B **61**, 422 (2000).

[21] Y. Moritomo, S. Xu, A. Machida, T. Akimoto, E. Nishibori, M. Takata, M. Sakata, and K. Ohoyama, J. Phys. Soc. Jpn. **69**, 1723 (2000).

[22] Y. Moritomo, H. Kusuya, T. Akimoto, and A. Machida, Jpn. J. Appl. Phys. **39**, L360 (2000).

[23] R. Gross, J. Klein, B. Wiedenhorst, C. Höfener, U. Schoop, J. B. Philipp, M. Schonecke, F. Herbstritt, L. Alff, Yafeng Lu, A. Marx, S. Schymon, S. Thienhaus, W. Mader, in *Superconducting and Related Oxides: Physics and Nanoengineering IV*, D. Pavuna and I. Bosovic eds., SPIE Conf. Proc. **4058** (2000), pp. 278–294.

[24] J. B. Philipp, D. Reisinger, M. Schonecke, A. Marx, A. Erb, L. Alff, and R. Gross, J. Appl. Phys. **93**, 6853 (2003).

[25] For a review see: J. B. Goodenough, J. M. Longo, in: K.-H. Hellwege, O. Madelung (Eds.), *Magnetic and Other Properties of Oxides and Related Compounds*, Landolt-Börnstein, New Series, Group III, vol. 4, Springer, Berlin, 1970.

[26] Y. Tokura and Y. Tomioka, J. Magn. Magn. Mater. **200**, 1 (1999).

[27] R. D. Shannon, Acta Cryst. A **32**, 751 (1976). We have used for alkaline rare earth elements coordination number 12, and for transition metals coordination number 6.

[28] M. Shikano, O. Ishiyama, Y. Inaguma, T. Nakamura, and M. Itoh, J. Solid State Chem. **120**, 238 (1995).

[29] M. W. Lufaso and P. M. Woodward, Acta Cryst. B **57**, 725 (2001).

[30] R. P. Borges, R. M. Thomas, C. Cullinan, J. M. D. Coey, R. Suryanarayanan, L. Ben-Dor, L. Pinsard-Gaudart, and A. Revcolevschi, J. Phys.: Condens. Matter **11**, L445 (1999).

[31] C. Ritter, M. R. Ibarra, L. Morellón, J. Blasco, J. García, and J. M. De Teresa, J. Phys.: Condens. Matter **12**, 8295 (2000).

[32] W. H. Song, J. M. Dai, S. L. Ye, K. Y. Wang, J. J. Du, and Y. P. Sun, J. Appl. Phys. **89**, 7678 (2001).

[33] Bog-Gi Kim, Yew-San Hor, and S-W. Cheong, Appl. Phys. Lett. **79**, 388 (2001).

[34] H. Y. Hwang, S-W. Cheong, P. G. Radaelli, M. Marezio, and B. Batlogg, Phys. Rev. Lett. **75**, 914 (1995).

[35] J. P. Zhou, J. T. McDevitt, J. S. Zhou, H. Q. Yin, J. B. Goodenough, Y. Gim, and Q. X. Jia, Appl. Phys. Lett. **75**, 1146 (1999).

[36] F. K. Patterson, C. W. Moeller, and R. Ward, Inorg. Chem. **2**, 196 (1963).

[37] A. Arulraj, K. Ramesha, J. Gopalakrishnan, and C. N. R. Rao, J. Solid State Chem. **155**, 233 (2000).

[38] A. W. Sleight, J. Longo, and R. Ward, Inorganic Chem. **1**, 245 (1962).

[39] M. Itoh, I. Ohta, and Y. Inaguma, Materials Science and Engineering B **41**, 55 (1996).

[40] G. Popov, M. Greenblatt, and M. Croft, Phys. Rev. B **67**, 024406 (2003).

[41] A. K. Azad, S. A. Ivanov, S.-G. Eriksson, J. Eriksen, H. Rundlöf, R. Mathieu, and P. Svedlindh, Materials Research Bulletin **36**, 2485 (2000).

[42] A. K. Azad, S. Ivanov, S. -G. Eriksson, H. Rundlöf, J. Eriksen, R. Mathieu, and P. Svedlindh, J. Magn. Magn. Mater. **237**, 124 (2001).

[43] A. K. Azad, S. A. Ivanov, S.-G. Eriksson, J. Eriksen, H. Rundlöf, R. Mathieu, and P. Svedlindh, Materials Research Bulletin **36**, 2215 (2000).

[44] J. M. Dai, W. H. Song, S. G. Wang, S. L. Ye, K. Y. Wang, J. J. Du, Y. P. Sun, J. Fang, J. L. Chen, and B. J. Gao, Materials Science and Engineering B **83**, 217 (2001).

[45] Ll. Balcells, J. Navarro, M. Bibes, A. Roig, B. Martínez, and J. Fontcuberta, Appl. Phys. Lett. **78**, 781 (2001).

[46] J. S. Park, B. J. Han, C. S. Kim, and B. W. Lee, J. Magn. Magn. Mater. **226-230**, 741 (2001).

[47] J. Gopalakrishnan, A. Chattopadhyay, S. B. Ogale, T. Venkatesan, R. L. Greene, A. J. Millis, and K. Ramesha, B. Hannoyer, and G. Marest Phys. Rev. B **62**, 9538 (2000).

[48] W. Westerburg, O. Lang, C. Ritter, C. Felser, W. Tremel, and G. Jakob, Solid State Comm. **122**, 201 (2002).

[49] W. Prellier, V. Smolyaninova, A. Biswas, C. Galley, R. I. Greene, K. Ramesha, and J. Gopalakrishnan, J. Phys.: Condens. Matter **12**, 965 (2000).

[50] H. Kato, T. Okuda, Y. Okimoto, Y. Tomioka, K. Oikawa, T. Kamiyama, and Y. Tokura, Phys. Rev. B **65**, 144404 (2002).

[51] A. K. Azad, S. -G. Eriksson, A. Mellergard, S. A. Ivanov, J. Eriksen, and H. Rundlöf, Materials Research Bulletin **37**, 1797 (2000).

[52] K.-I. Kobayashi, T. Okuda, Y. Tomioka, T. Kimura and Y. Tokura, J. Magn. Magn. Mater. **218**, 17 (2000).

[53] F. S. Galasso, *Structure, Properties and Preparation of Perovskite-Type Compounds* (Pergamon, London, 1969).

[54] M. Imada, A. Fujimori, and Y. Tokura, Rev. Mod. Phys. **30**, 1039 (1998).

[55] A. Ogale, S. Ogale, R. Ramesh, and T. Venkatesan, Appl. Phys. Lett. **75**, 537 (1999).

[56] M. T. Anderson, K. B. Greenwood, G. A. Taylor, and K. R. Poeppelmeier, Prog. Solid State Chem. **22**, 197 (1993).

[57] T. Saha-Dasgupta, and D. D. Sarma, Phys. Rev. B **64**, 064408 (2001).

[58] Horng-Tay Jeng, and G. Y. Guo, Phys. Rev. B **67**, 094438 (2003).

[59] O. K. Anderson, and O. Jepsen, Phys. Rev. Lett. **53**, 2571 (1984).

[60] O. K. Andersen and O. Jepsen, and D. Glotzel, in *Highlights of Condensed-Matter Theory*, edited by F. Bassani, F. Fumi, and M. P. Tosi (North-Holland, Amsterdam, 1985).